Mode transition in homogenous dielectric barrier discharge in argon at atmospheric pressure*

Liu Fu-Cheng(刘富成)†, He Ya-Feng(贺亚峰), and Wang Xiao-Fei(王晓菲)

Hebei Key Lab of Optic-Electronic Information and Materials, College of Physics Science and Technology, Hebei University, Baoding 071002, *China*

(Received 21 December 2013; revised manuscript received 23 January 2014; published online 22 May 2014)

The influence of driving frequency on the discharge regime of a homogenous dielectric barrier discharge in argon at atmospheric pressure is studied through a one-dimensional self-consistent fluid model. The simulation results show that the discharge exhibits five notable discharge modes, namely the Townsend mode, stable glow mode, chaotic mode, asymmetric glow, and multiple period glow mode in a broad frequency range. The transition mechanisms of these modes should be attributed to the competition between the applied voltage and the memory voltage induced by the surface charges.

Keywords: Townsend mode, glow mode, mode transition, fluid model

PACS: 52.80.Hc, 52.65.–y. 52.20.–j **DOI:** 10.1088/1674-1056/23/7/075209

1. Introduction

In recent years, non-equilibrium atmospheric pressure plasmas have attracted much attention due to their unique features including chamber-free operation and enhanced chemistry without elevated gas temperature.[1,2] These attractive features make them suitable for a broad prospect in industrial and biomedical applications, such as thin film deposition, surface modification, ozone generation, bio-sterilization, and so on.[3–5] One of the promising non-equilibrium plasma sources is the dielectric barrier discharge (DBD). Although DBD usually operate in a filamentary form at atmospheric pressure, however, it also can exhibit a homogeneous diffuse mode under certain conditions, which is called the atmospheric pressure glow discharge (APGD).[6] During the past decades, the homogenous DBDs at atmospheric pressure have been obtained in helium, argon, nitrogen, neon, and their mixtures.[7–10]

There have been a great number of papers concerning the characteristics of APGDs, especially the discharge modes and their transitions.[6,10–16] Two homogenous modes, named as the Townsend mode and glow mode, were discovered in helium.[6] Radu *et al.*[11] experimentally showed that the discharge mode is related directly to the power frequency. Lee *et al.*[12] studied the mode transition between these two modes in helium and oxygen mixture using a one-dimensional (1D) fluid model and found that it was a Townsend discharge for low frequency but a glow discharge for the higher frequency. Similar simulation results have been also found in pure helium by two-dimensional fluid models.[13] It is experimentally observed that asymmetric pulsed phenomena were presented in the dielectric barrier glow discharge in helium.[5,14] Ha *et al.*[15] found that the glow mode and the Townsend mode could coexist in the asymmetric discharge. Wang and collaborators[16] demonstrated that a glow discharge can transit into a chaotic mode or a periodic mode with multiple periods by double period bifurcation. Zhang *et al.*[17] found that an asymmetric mode exists between the symmetric glow mode and the period-two glow mode. In spite of the great efforts that have been made on these problems, studies of the transition mechanisms among these discharge modes have so far not been systematic.

Most numerical modeling work has concentrated on the mode transitions in helium gas discharge while attention on the argon discharge is not as extensive.[18,19] Thus, the aim of this paper is to develop a self-consistent 1D fluid model for the mode transitions in homogenous dielectric barrier discharge in argon at atmospheric pressure. Our simulation results show that the discharge transits from the Townsend discharge to the glow discharge, and then to the chaotic mode, asymmetric glow mode, symmetric glow mode, and multiple period glow mode by increasing the external frequency in a broad range (from kHz to MHz).

2. Model description

The discharge occurs between two parallel-plate electrodes covered by dielectric layers ($\varepsilon_r = 9$) of 1-mm thickness. One electrode is grounded and the other is driven by a sinusoidal excitation voltage, whose repetitive frequency can range from 1 kHz to several tens of MHz. The width of the electrodes is fixed, while their length is assumed to be infinite. No external circuit is included.

Pure argon is taken as the working gas. Five chemical

*Project supported by the National Natural Science Foundation of China (Grant No. 11205044), the Hebei Natural Science Fund, China (Grant Nos. A2012201015 and A2011201006), the Research Foundation of Education Bureau of Hebei Province, China (Grant No. Y2012009), and the Postdoctoral Science Foundation and Foundation of Hebei University, China (Grant No. 2010Q30).

†Corresponding author. E-mail: hdlfc@hbu.cn

© 2014 Chinese Physical Society and IOP Publishing Ltd

species are considered: electrons (e); argon atom metastable (Ar^*); argon molecule metastable (Ar_2^*); singly charged argon positive ion (Ar^+); and argon molecular ion (Ar_2^+). The pressure and the temperature of the background argon gas are assumed to be 1 atm and 300 K, respectively. We employed a one-dimensional fluid model with the local field approximation (LFA). The continuity equations for electron, ions, and metastables are

$$\frac{\partial n_i}{\partial t} + \frac{\partial \Gamma_i}{\partial x} = S_i, \tag{1}$$

$$\Gamma_i = \mathrm{sgn}(q_i)\mu_i n_i E - D_i \frac{\partial n_i}{\partial x}, \tag{2}$$

where subscript i indicates the i-th species, n_i is the density, Γ_i is the flux in the drift-diffusion approximation, S_i is the net creation rate for species i, q_i is the charge, μ_i and D_i are the mobility and diffusion coefficients, whose values are identical to those used in Refs. [20] and [21], and E is the electric field. The equations system is closed by Poisson's equation

$$\varepsilon_0 \nabla^2 V = -\varepsilon_0 \nabla \cdot \boldsymbol{E} = -e\sum_i q_i n_i, \tag{3}$$

where V, ε_0, and e are the potential, permittivity in a vacuum, and electron charge, respectively. All the chemical reactions and reaction rate coefficients used in the present model are listed in Table 1, most of which are taken from the literature.[22–25]

Table 1. Elementary reaction processes with their reaction rate coefficients in argon discharge. The first three reactions are all calculated using the external Boltzmann solver Bolsig+.[22]

Number	Reaction	Reaction coefficient	Ref.
R1	$e + Ar \rightarrow e + Ar^*$	$f(E/N)$	[22]
R2	$e + Ar \rightarrow 2e + Ar^+$	$f(E/N)$	[22]
R3	$e + Ar^* \rightarrow 2e + Ar^+$	$f(E/N)$	[22]
R4	$e + Ar^* \rightarrow e + Ar$	$4.3\times10^{-10}T_e^{0.74}$	[23]
R5	$Ar^* + Ar^* \rightarrow e + Ar^+ + Ar$	5.0×10^{-10}	[24]
R6	$e + Ar^+ \rightarrow Ar^*$	$4.0\times10^{-13}T_e^{-0.5}$	[25]
R7	$2e + Ar^+ \rightarrow e + Ar^*$	$5.0\times10^{-27}T_e^{-4.7}$	[25]
R8	$e + Ar_2^+ \rightarrow Ar^* + Ar$	$5.38\times10^{-8}T_e^{-0.66}$	[25]
R9	$Ar_2^* + Ar_2^* \rightarrow e + 2Ar + Ar_2^+$	5.0×10^{-10}	[25]
R10	$Ar^* + 2Ar \rightarrow Ar_2^* + Ar$	1.14×10^{-32}	[25]
R11	$Ar^+ + 2Ar \rightarrow Ar_2^+ + Ar$	2.5×10^{-31}	[25]
R12	$Ar_2^* \rightarrow 2Ar + hv$	$6.0\times10^{7}\,s^{-1}$	[25]
R13	$e + Ar_2^* \rightarrow 2e + Ar_2^+$	$9.0\times10^{-8}T_e^{0.7}\exp(-3.66/T_e)$	[25]
R14	$e + Ar_2^* \rightarrow e + 2Ar$	1.0×10^{-7}	[25]

Note: two-body reactions are in units of $cm^3\cdot s^{-1}$; three-body rates are in units of $cm^6\cdot s^{-1}$.

The total electric current density j_0 in the discharge region is found by Sato's equation with the time-dependent applied voltage

$$j_0 = \left(\frac{2d_m}{\varepsilon_r} + d_g\right)^{-1}\left[\int_0^{d_g} i_c(x,t)\,dx - \varepsilon_0\frac{\partial V_a}{\partial t}\right], \tag{4}$$

where d_g and d_m are the thickness values of the discharge gap and the dielectric barrier layer; V_a is the applied voltage, and $i_c(x,t)$ is the conduction current density.

The boundary conditions for Eqs. (1) and (2) used in this study is that at the anode, the ion density should be zero while at the cathode, the secondary electron emission $\gamma_e = 0.01$ from the dielectrics through ion impact was taken into account. As for the boundary condition for Poisson' equation, it is given in terms of the electric fields at the interface between the gas gap and the dielectric barrier

$$\varepsilon_r\varepsilon_0 E_{dielec} + \sigma_0 = \varepsilon_0 E_{plasma}, \tag{5}$$

where ε_r is the relative dielectric constant of the dielectrics and σ_0 is the surface charge density accumulated on the dielectric barriers.

3. Results and discussion

The simulation parameters are chosen as follows: the discharge gap d_g is fixed to 1 mm; the amplitude of the applied voltage is 1.5 kV; the gas pressure is 10^5 Pa; the gas temperature is set to 300 K while the electron temperature is set to 1.5 eV; the initial value of electron density is taken as 10^7 cm^{-3}, and argon metastable density and argon excimer molecule density are 10^2 cm^{-3}; and the initial densities of the two argon ions are half of the value of electron density for charge neutrality. Under these conditions, the discharge is uniform and only one current pulse can be formed in every half-cycle in all cases. It should be noted that the initial particle densities just affect the onset time of the first gas breakdown. A smaller initial density requires a longer time to build up sufficient electrons for the initiation of the discharge. A stable discharge is reached typically 5–10 ac cycles after the first breakdown.

In order to check the validation of our model, in Fig. 1, we present a direct comparison between the experimental data[26] and our simulation results for V–I characteristics of a 1.1-mm

gap APGD with a 5.2-kHz driving frequency and a 2.25-kV peak external voltage. The amplitude of the current pulse peak is about 6 mA in the experiment and is well predicted by the computational model. This indicates that our model is capable of accurately capturing the main features of APGDs in argon at atmospheric pressure.

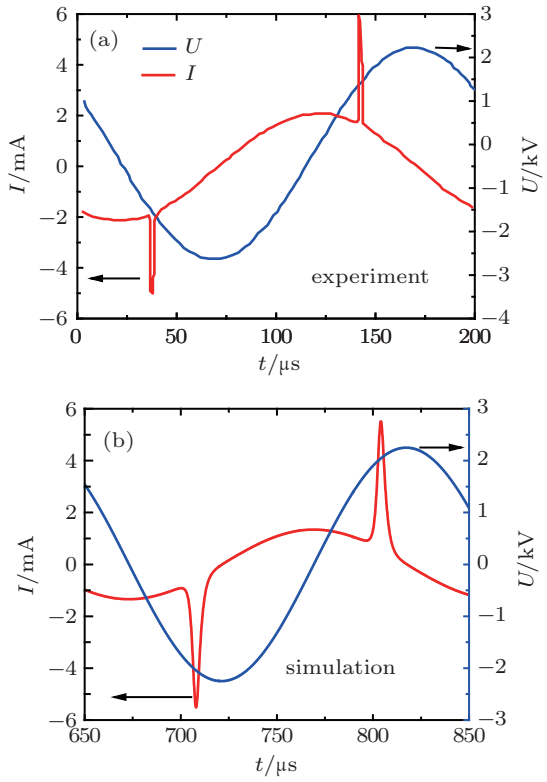


Fig. 1. (color online) Comparison of experimental data and simulation results for atmospheric pressure glow discharge V–I waveforms in pure argon for a 1.1-mm gap with 5.2 kHz and 2.25 kV driving amplitude. The thickness of dielectric layers ($\varepsilon_r = 4$) are 2.1 mm.

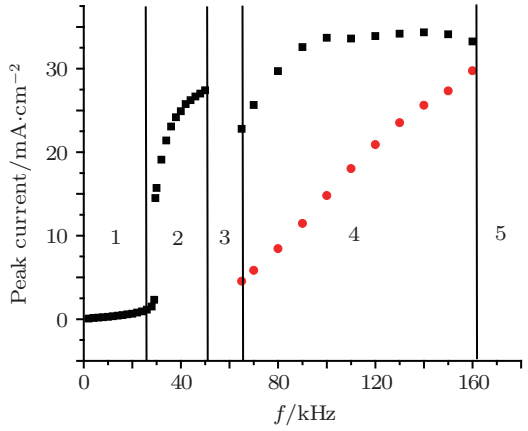


Fig. 2. (color online) Peak current density of discharge pulses as a function of the driving frequency. Number 1 means Townsend mode; number 2: stable glow mode; number 3: chaotic mode; number 4: asymmetric mode; number 5: multiple period mode.

Taking the driving frequency as the control parameter, we investigate the discharge characteristics and mode transitions in the homogenous dielectric barrier discharge in argon at atmospheric pressure. Figure 2 gives the peak current as a function of the driving frequency. It is demonstrated that the variation of peak current exhibits different behaviors in different ranges of frequency. There are five distinct frequency ranges in which the discharge operates in different modes. As will be described in more detail below, the five discharge modes are the Townsend mode, stable glow mode, chaotic mode, asymmetric glow mode, and multiple-period glow mode, respectively.

Figures 3(a)–3(c) show voltage–current characteristics and the corresponding distributions of the charged particles and the electric field at the peak current for 10 kHz, 29 kHz, and 40 kHz external driving frequencies. It is clearly seen that the magnitude of the current density increases as the driving frequency increases. When the driving frequency is set to 10 kHz, the peak current density is very small (about 0.28 mA/cm^2), and the current profile is not peaked, rather it spreads broadly, as in Fig. 3(a). The full width at half maximum of this current pulse is about 13.2 μs. Note that the instantaneous cathode locates at $x = 0$ mm and the anode locates at $x = 1$ mm. The electron density rises monotonously from the cathode to the anode and its highest value is on the order of 10^8 cm^{-3}, while the highest ion density is about 3.9×10^{10} cm^{-3}. The electric field is increased almost linearly and no quasi-neutral plasma region is formed. These behaviors indicate that this discharge is operating in the Townsend mode.[27] As the driving frequency is increased to 29 kHz, the peak current density is gradually increased to 2.31 mA/cm^2 and the current profile becomes pulsed. The maximal electron density is located near the anode, but the maximal ion density is located slightly apart from the cathode, as shown in Fig. 3(b). When the driving frequency is larger than 29.1 kHz, the peak current density increases dramatically and the discharge transits from the Townsend mode to a glow mode. The major feature of this discharge mode is the formation of the cathode fall region and a positive column region, as shown in Fig. 3(c). Similar results have also been found both in experiments[11] and in simulations.[12,13]

When the driving frequency exceeds 51 kHz, the stable glow discharge becomes unstable and transits into a chaotic discharge mode. In Fig. 4, we present the current characteristics and its corresponding current–voltage relationship for a slightly higher driving frequency, which leads to the appearance of the chaotic mode. One can see that the discharge current pulses in this mode are no longer periodic and the current peak fluctuates stochastically. It is worth pointing out that the phase space in Fig. 4(b) contains data of 50 cycles of the applied voltage and each discharge in the half cycle has its own trajectory. The effects of the frequency increase on the mode transition from the glow mode to a chaotic mode can be interpreted in terms of the competition between the applied voltage V_a and the memory voltage V_m induced by charge accumulation on the dielectric surface. The gas voltage V_g across the gas

gap is determined by these two voltages, i.e., $V_g = V_a - V_m$. Once the gas voltage reaches the breakdown voltage V_b, the gas is ignited. The produced electrons accumulating on the dielectric result in the increase of the memory voltage and make the gas voltage collapse abruptly to some residual voltage V_r, as shown in Fig. 4(c). When the driving frequency is low, there is enough time for electrons to drift to the anode and accumulate on the dielectric surface. As the frequency is increased, the increase of applied voltage becomes faster while the memory voltage becomes slower because the drift time of electrons becomes shorter, resulting in the increase of the gas voltage that determines the ionization level. This is the reason why the discharge current increases as the driving frequency is increased. When the frequency is too high, it is possible that some electrons will be unable to reach the electrodes and the memory voltage cannot be increased adequately. This makes it impossible to sustain a stable glow discharge.

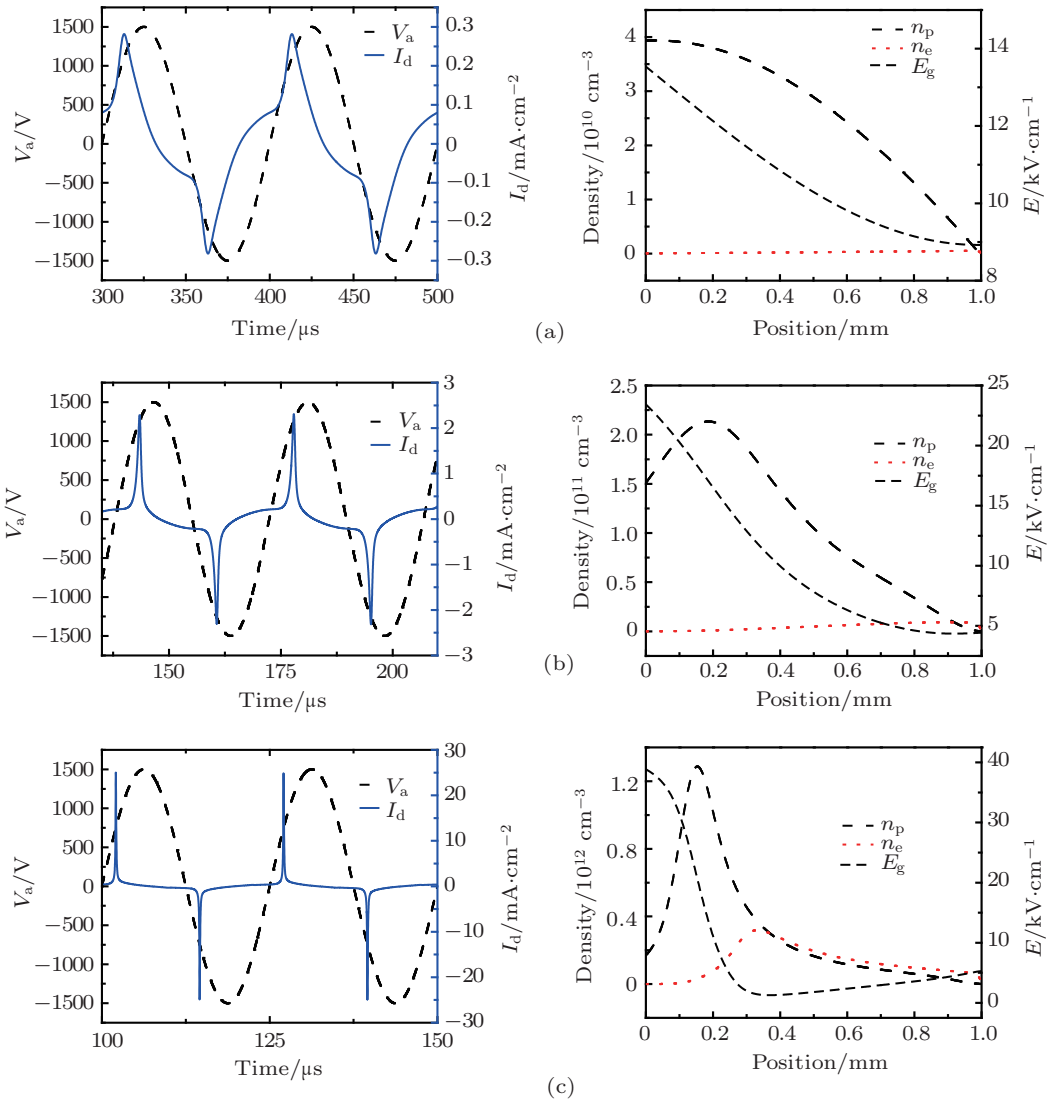


Fig. 3. (color online) Simulation results for voltage–current characteristics and the corresponding distributions of charged particles and electric field at the peak current for different external driving frequencies. (a) $f = 10$ kHz; (b) $f = 29$ kHz; and (c) $f = 40$ kHz. Instantaneous cathode locates at $x = 0$ mm.

In order to evaluate this hypothesis, the breakdown voltage V_b, residual voltage V_r, as well as the corresponding voltage difference $\Delta V = V_b - V_r$ in the stable glow mode as a function of the excitation frequency is presented in Fig. 5. It is found that the breakdown voltage remains unchanged while the residual voltage decreases as the frequency increases. The corresponding voltage difference gradually increases when the surface charges can alter the memory voltage adequately. However, if the frequency is large enough, the short drift time of electrons makes the memory voltage unable to change sufficiently. In addition, the quasi-neutral plasma produced during the previous breakdown is not completely destructed because of the higher frequency.[27] The abundant residual charged particles can serve as the seed electron and give rise to a lower breakdown voltage in the successive discharge. Therefore, the voltage difference begins to decrease, as shown in the inset

enlarged photograph in Fig. 5.

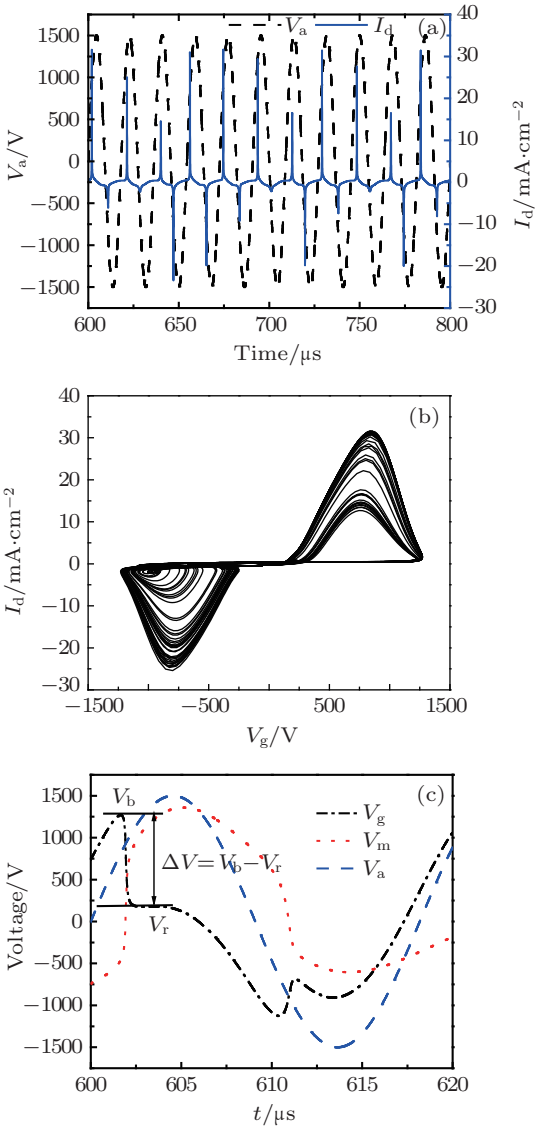


Fig. 4. (color online) Discharge characteristics in a chaotic mode with the driving frequency $f = 55$ kHz. Voltage–current characteristics (a) and the corresponding trajectory in phase space (b). (c) The time evolutions of the applied voltage, gas voltage, and the memory voltage.

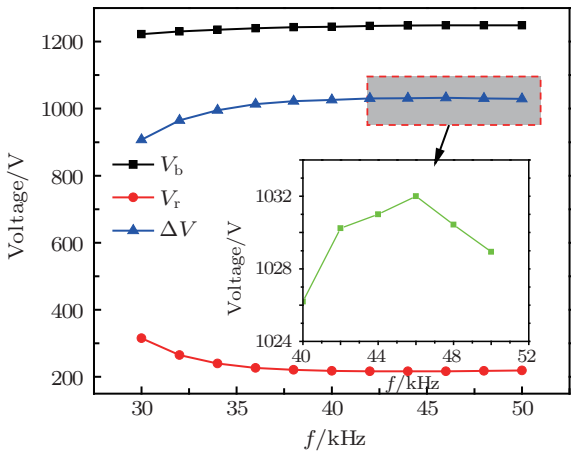


Fig. 5. (color online) The influence of driving frequency on the breakdown voltage, residual voltage, as well as the voltage difference.

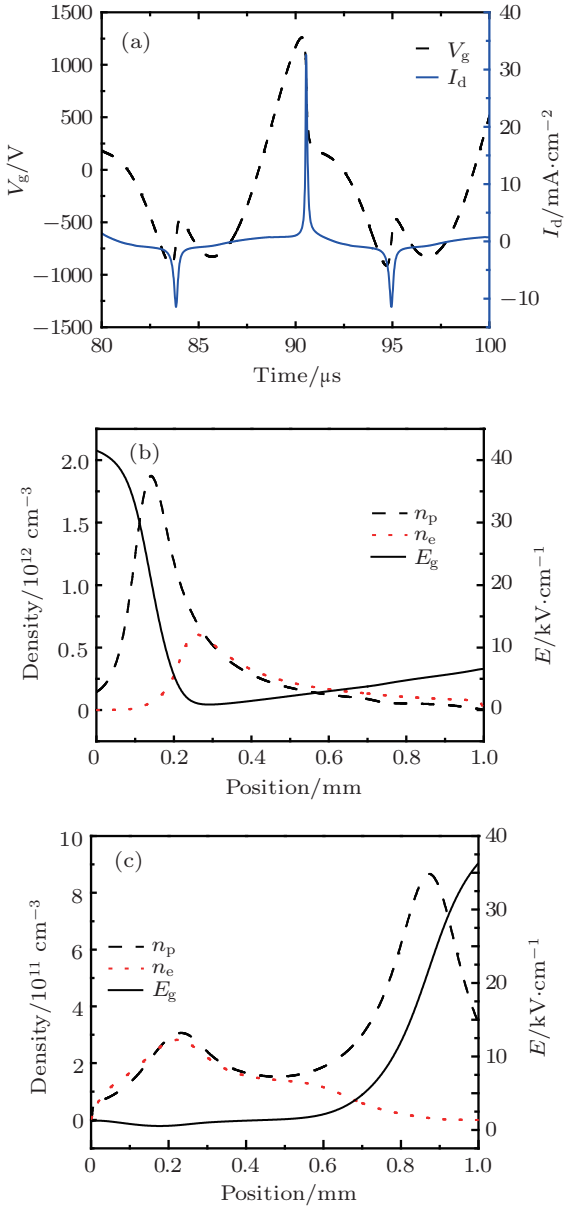


Fig. 6. (color online) (a) Voltage–current characteristics for asymmetric modes and the corresponding distributions of charged particles and electric field at the peak current for the positive pulse (b) and the negative pulse (c), respectively. The driving frequency is 90 kHz. The instantaneous cathode locates at $x = 0$ mm in panel (b) and at $x = 1$ mm in panel (c).

The discharge transits into an asymmetric glow mode if the driving frequency is further increased. Figures 6(a)–6(c) show the discharge properties in the asymmetric mode with the driving frequency $f = 90$ kHz. In Fig. 6(a), the discharge current and the gas voltage across the gas gap are plotted as a function of time. One can see that the amplitude of the current pulse in the positive half cycle is much larger than that in the negative half cycle. It should be noted that the choice of larger pulse depends on the initial phase of the applied voltage and reverses if the initial phase shifts half cycle. Figures 6(b) and 6(c) present the spatial distributions of electron density, ion density, as well as electric field at the peak current for the positive and the negative pulses, respectively. The instantaneous cathode locates at $x = 0$ mm in Fig. 6(b) and at $x = 1$ mm in

Fig. 6(c). It is obvious that both of the discharges are operating in the glow mode for the formation of the cathode fall and the positive column region. The biggest difference between these two patterns is that the residual charged particles in the negative discharge pulse still remains 3.2×10^{11} cm^{-3} near the momentary anode. These high concentrations of ions and electrons result mainly from the positive discharge pulse. Such spatial density distributions would influence the characteristics of the negative discharge. The dependence of the peak current density for both discharge pulses on the driving frequency is shown in Fig. 2. It is seen that the peak current of positive and negative discharge vary with frequency quite differently. While at positive polarity, the amplitude changes rather slowly, at negative polarity, a dramatic increase with frequency takes place. When the two peak current densities become nearly equal, the asymmetric discharge undergoes a transition into a multiple period discharge mode.

Figures 7(a)–7(c) show the time evolutions of the discharge current and the gas voltage for 200 kHz, 400 kHz, and 10 MHz external driving frequencies. Figure 7(a) shows the discharge bifurcates into a period-3 state, in which the discharge current pulses repeat every three cycle of the applied voltage. In Fig. 7(b), the discharge operates in a period-2 state. The maximum of the peak current density increase as the frequency is increasing. The intrinsic feature of multiple-period discharge has been confirmed experimentally in a helium discharge.[28] When the frequency is high enough, a stable symmetric discharge with similar characteristics to the radiofrequency discharge takes place, as shown in Fig. 7(c). The formation of this symmetric discharge can be interpreted by the electron trapping mechanism. At atmospheric pressure, the amplitude of electron oscillatory displacement $r_{\max}$ can be approximated by $r_{\max} = eE_a/m_e\omega\nu_m$ because $\nu_m \gg \omega$.[29] Here, $\omega = 2\pi f$ is the angular frequency, E_a is the amplitude of the electric field, m_e is the electron mass, and ν_m is the effective collision frequency of electrons. It can be reduced to $r_{\max} = \langle\mu_e\rangle E_a/\omega$ in terms of the average electron mobility $\langle\mu_e\rangle$ over the time varying electric field. If this displacement is less than $d_g/2$, few electrons can reach the dielectric surface. In other words, electrons are trapped in the gas gap. In this situation, the effects of the memory voltage can be negligible and the discharge is mainly determined by the applied voltage. In our simulations, $\langle\mu_e\rangle$ is equal to 394 cm$^2 \cdot$ V$^{-1} \cdot$ s^{-1}, $E_a = 6.5$ kV/cm, so the corresponding frequency is 8 MHz. This value is comparable to the simulated value of 10 MHz.

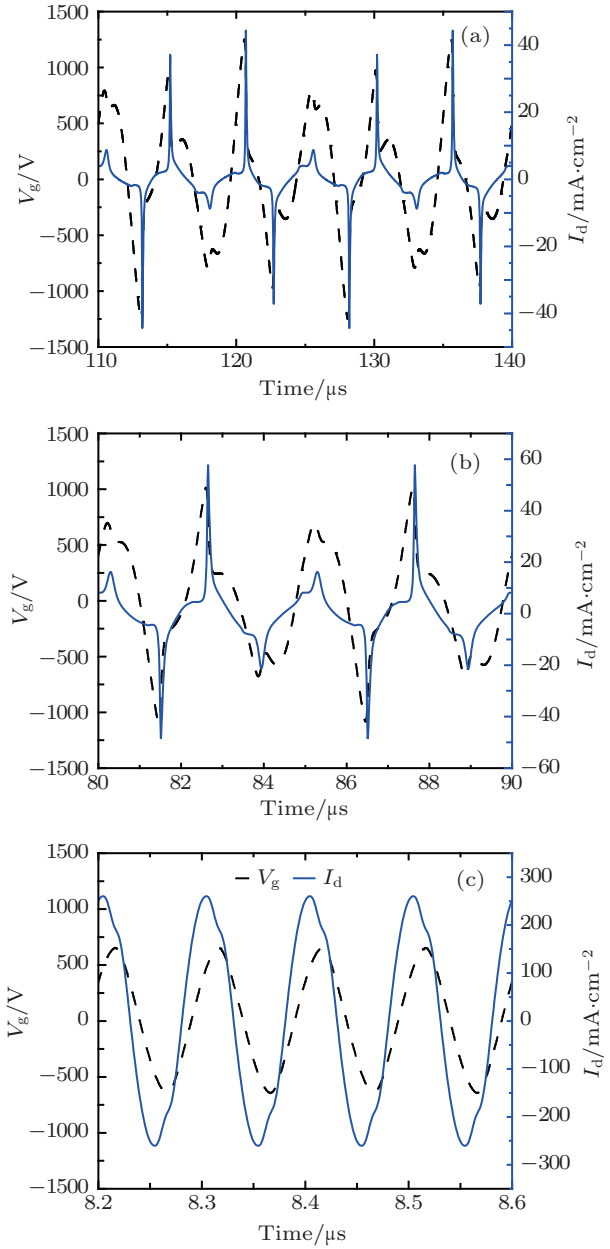


Fig. 7. (color online) Time evolutions of the current density and the gas voltage at different driving frequencies. (a) $f = 200$ kHz; (b) $f = 400$ kHz; (c) $f = 10$ MHz.

4. Conclusions

In this paper, we presented a numerical description of the discharge characteristics and mode transitions of homogenous dielectric barrier discharge in argon at atmospheric pressure. Five operating modes, namely Townsend, stable glow, chaotic mode, asymmetric glow, and multiple-period glow mode, have been observed under different frequency ranges. The competition between the applied voltage and the memory voltage is responsible for the mode transitions. When the driving frequency is very low, the discharge operates in the Townsend mode. As the frequency is increasing, the increase of the applied voltage becomes faster while the memory voltage becomes slower because the drift time of electrons becomes shorter. The mismatch between these two voltages gives rise

to the higher ionization level and larger current density. The discharge gradually transits into a glow mode. When the memory voltage cannot be changed adequately because of the short transiting time, the glow mode becomes unstable and transits into an asymmetric glow mode through a chaotic stage. When the two peak current densities become nearly equal, the asymmetric discharge undergoes a transition into a multiple-period discharge mode. If all electrons are trapped in the gas gap, a symmetric glow discharge with a single period takes place.

References

[1] Liu F C, Yan W and Wang D Z 2013 *Acta Phys. Sin.* **62** 175204 (in Chinese)

[2] Liu X H, He W, Yang F, Wang H Y, Liao R J and Xiao H G 2012 *Chin. Phys. B* **21** 075201

[3] Park G Y, Park S J, Choi M Y, Koo I G, Byun J H, Hong J W, Sim J Y, Collins G J and Lee J K 2012 *Plasma Sources Sci. Technol.* **21** 043001

[4] Roth J R, Rahel J, Dai X and Sherman D M 2005 *J. Phys. D: Appl. Phys.* **38** 555

[5] Dai D, Wang Q M and Hao Y P 2013 *Acta Phys. Sin.* **62** 135204 (in Chinese)

[6] Massines F, Rabehi A, Decomps P, Gadri R B, Segur P and Mayoux C 1998 *J. Appl. Phys.* **83** 2950

[7] Okazaki S, Kogoma M, Uehara M and Kimura Y 1993 *J. Phys. D: Appl. Phys.* **26** 889

[8] Merbahi N, Sewraj N, Marchal F, Salamero Y and Millet P 2004 *J. Phys. D: Appl. Phys.* **37** 1664

[9] Trunec D, Brablec A and Buchta J 2001 *J. Phys. D: Appl. Phys.* **34** 1697

[10] Massines F, Gherardi N, Naude N and Segur P 2009 *Eur. Phys. J. Appl. Phys.* **47** 22805

[11] Radu I, Bartnikas R and Wertheimer M R 2003 *IEEE Trans. Plasma. Sci.* **31** 1363

[12] Lee D, Park J, Hong S and Kim Y 2005 *IEEE Trans. Plasma. Sci.* **33** 949

[13] Wang Q, Sun J Z and Wang D Z 2011 *Phys. Plasmas* **18** 103504

[14] Shin J and Raja L L 2007 *J. Phys. D: Appl. Phys.* **40** 3145

[15] Ha Y, Wang H J and Wang X F 2012 *Phys. Plasmas* **19** 012308

[16] Wang Y H, Zhang Y T, Wang D Z and Kong M. G 2007 *Appl. Phys. Lett.* **90** 071501

[17] Zhang D Z, Wang Y H and Wang D Z 2013 *Phys. Plasmas* **20** 063504

[18] Zhang Z H, Shao X J, Zhang G J, Li Y X and Peng Z Y 2012 *Acta Phys. Sin.* **61** 045205 (in Chinese)

[19] Shkurenkov I A, Mankelevich Y A and Rakhimova T V 2011 *Eur. Phys. J. D* **61** 95

[20] Li Z, Zhao Z and Li X H 2013 *Phys. Plasmas* **20** 013503

[21] Richards A D, Thompson B E and Sawin H H 1987 *Appl. Phys. Lett.* **50** 492

[22] Hagelaar G J M and Pithford L C 2005 *Plasma Sources Sci. Technol.* **14** 722

[23] Zhang Y R, Xu X and Wang Y N 2010 *Phys. Plasmas* **17** 033507

[24] Balcon N, Hagelaar G J M and Boeuf J P 2008 *IEEE Trans. Plasma Sci.* **36** 2782

[25] Deconinck T and Raja L L 2009 *Plasma Process. Polym.* **6** 335

[26] Kloc P, Wagner H E, Trunec D, Navratil Z and Fedpseev G 2010 *J. Phys. D: Appl. Phys.* **43** 345205

[27] Golubovskii Y B, Maiorov V A, Behnke J and Behnke J F 2003 *J. Phys. D: Appl. Phys.* **36** 39

[28] Wang X Q, Dai D, Hao Y P and Li L C 2012 *Acta Phys. Sin.* **61** 230504 (in Chinese)

[29] Shi J J, Deng X T, Hall R, Punnett J D and Kong M G 2003 *J. Appl. Phys.* **94** 6303